Jurnal Tribologi 47 (2025) 227-248

MYTRIBOS Malaysian Tribology Society

Jurnal Tribologi

Website : jurnaltribologi.mytribos.org e-issn: 2289-7232

Numerical analysis of AISI 4340 steel machinability under high-speed turning conditions

Haniff Abdul Rahman [1*], Jaharah A Ghani [1], Mohd. Rasidi Mohd. Rasani [1], Saima Yaqoob [1], Khairul Aiman Khairul Anuar [2]

[1] Department of Mechanical and Manufacturing Engineering, Faculty of Engineering and Built Environment, Universiti Kebangsaan Malaysia, MALAYSIA.
[2] CADIT Consultants Malaysia Sdn Bhd, MALAYSIA.
*Corresponding author: p119248@siswa.ukm.edu.my

KEYWORDS

FEA
AISI 4340
HSM
Turning

ABSTRACT

This study investigates the machining challenges of AISI 4340 steel, a material highly utilized in heavy industries for its strength and wear resistance but difficult to machine due to hardness, high tensile strength, and poor thermal conductivity. While High-Speed Machining (HSM) offers potential productivity benefits, heat generation at speeds above 300 m/min remains a key issue that shortens tool life. Existing research has also not sufficiently explored machinability at cutting speeds up to 400 m/min combined with very low feed rates. To address this, Finite Element Analysis (FEA) was performed using ANSYS Explicit Dynamic to simulate turning operations on AISI 4340 steel at speeds from 300 to 400 m/min. Key factors such as cutting force and temperature at the tool-chip interface were analyzed relative to machining parameters. The findings reveal cutting speed mainly affects cutting temperature, while feed rate and depth of cut mainly influences cutting force. Cutting force results qualitatively matched prior experimental data trends, while the highest cutting temperature under highest speed also correlates with the shortest tool life. This work offers critical insights into machining behavior for understudied high-speed conditions, supporting efforts to optimize tool life and develop effective strategies for sustainable machining of AISI 4340 steel.

Received 7 August 2025; received in revised form 24 October 2025; accepted 27 October 2025.
To cite this article: Rahman et al. (2025). Numerical analysis of AISI 4340 steel machinability under high-speed turning conditions. Jurnal Tribologi 47, pp.227-248.

1.0 INTRODUCTION

AISI 4340 steel is a heat-treatable, medium-carbon, low-alloy steel known for its high toughness, good ductility, and low brittleness when properly heat-treated. In hardened condition, AISI 4340 steel offers excellent impact, wear and abrasion resistance making it a significantly ideal material for a wide range of industrial applications, particularly in the automotive and aerospace sectors for the manufacture of crankshafts, piston connecting rods, aircraft components, and valves (Azaath et al., 2020; Iynen et al., 2021; Natasha et al., 2016). A substantial portion of the production costs for components made from AISI 4340 steel is related to machining, owing to the material's high strength and hardness at elevated temperatures, which collectively contribute to its classification as a difficult-to-machine alloy (Guo & Yen, 2004; Konde, 2004).

The machining process aims to produce high dimensional accuracy products, desired surface finishes, at minimal costs. Figure 1 shows a schematic representation of the machining process using a single point cutting tool also known as the turning process, highlighting the three main cutting parameters: cutting speed, feed and depth of cut. Machining involves the use of a cutting tool to remove small chips of material from a workpiece, shaping it to precise specifications (Das et al., 2013). During this process, significant friction is generated at deformation zone as shown in Figure 2. Heat generation during the cutting process primarily arises from plastic deformation in the primary shear zone, friction at the tool–chip interface, and friction between the tool flank and the newly machined surface, with the majority of heat produced in the secondary zone at the tool–chip interface. Key factors influencing heat generation include cutting parameters such as speed, feed rate, depth of cut, and tool geometry, as well as workpiece and tool material properties and the use of lubrication or coolant systems. Typically, about 80% of the generated heat is removed by the chip, while 10% is absorbed by the cutting tool and another 10% by the workpiece, with the highest temperatures occurring where chip friction is most intense.

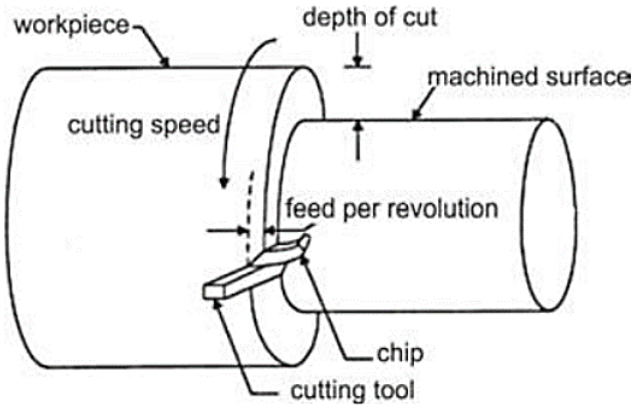

Figure 1: Schematic representation of machining process. Adapted after (Yang & Tarng, 1998).

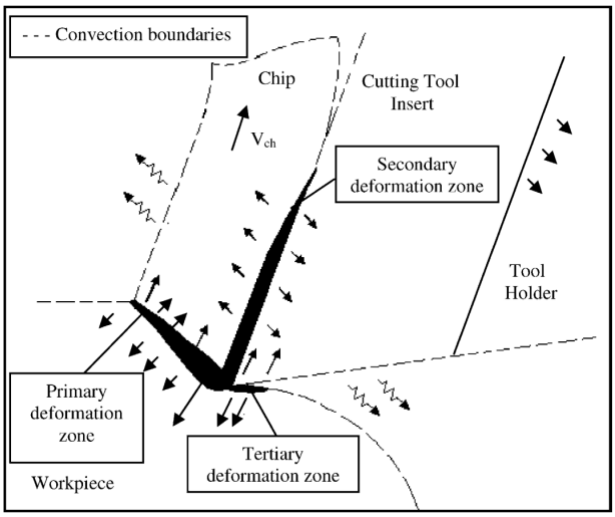

Figure 2: Schematic diagram of deformation zones linked to heat generation in machining. Adapted after Abukhshim et al., (2006).

The heat generated during machining can impact the accuracy of the process, as high temperatures particularly at the tool-chip interface can lead to tool wear, shortened tool life, compromised surface integrity of the workpiece, and altered chip formation mechanisms (Abukhshim et al., 2006; Chinchanikar & Choudhury, 2014). Excessive heat can also cause plastic deformation of the tool edge, adversely affecting the final accuracy of the workpiece (Shalaby & Veldhuis, 2018). Previous studies show that very high, localized temperatures occur at the tool–chip interface and in the primary shear zone. The predicted temperatures typically range from about 420–500 °C at the low end but can rise much higher, up to over 1000 °C depending on cutting conditions (Konde, 2004). Cutting speed and feed rate are primary factors controlling temperature in the cutting zone, with higher values directly leading to higher temperatures. Controlling cutting temperatures in the deformation zone is hence essential to minimize changes in the microstructure of the workpiece material, where effective cooling and lubrication strategy is typically crucial and can be costly.

High-speed machining (HSM) offers several advantages when working with hardened AISI 4340 steels by employing significantly higher cutting speeds than conventional machining often above 100 m/min. HSM notably reduces machining forces due to localized heating in the primary shear zone, which induces thermal softening and lowers flow stress, thereby enhancing workpiece accuracy by minimizing deflection (Al-Ghamdi & Iqbal, 2015). Additionally, HSM generally improves the surface finish of AISI 4340 steel, as lower cutting forces and enhanced chip flow promote smoother surfaces (Natasha et al., 2018). The process also allows for substantially higher material removal rates, leading to increase productivity. Moreover, HSM can potentially eliminate the need for grinding operations, resulting in significant cost savings, particularly when machining complex shapes (Naigade et al., 2013; Sahoo & Sahoo, 2012).

Despite its advantages, HSM also presents several challenges directly related to cutting parameters. Cutting speed significantly affects both surface finish and tool wear. While higher speeds generally enhance surface finish, it can also accelerate tool wear (Ahmad, Ghani, & Che Haron, 2022; Bag et al., 2022; Wagri et al., 2023). Feed rate is also crucial for surface roughness,

with higher rates typically increasing the roughness (Ahmad et al., 2021; Bag et al., 2020; da Silva et al., 2020). Meanwhile depth of cut has a lesser effect on surface roughness compared to cutting speed and feed rate, however increasing it can raise machining forces, potentially reducing tool life (Tiwari et al., 2020). The impact of these parameters can vary based on factors such as tool type, coating, and cooling methods. For instance, Chemical Vapor Deposition (CVD) coated tools is found to perform better than Physical Vapor Deposition (PVD) coated tools at higher speeds (Bag et al., 2020), and minimum quantity lubrication (MQL) can lower cutting temperatures and extend tool life (Ahmad, Ghani, & Haron, 2022).

In a recent study using Taguchi S/N ratio for response optimization when machining AISI 4340 steel at high speed regime, it was found that feed rate and cutting speed are both influential for tool life, while surface roughness are mainly influenced by the feed rate (Yaqoob, Ghani, Jouini, Juri, et al., 2024). This is supported with subsequent studies by (Jouini et al., 2025), which revealed that feed rate was the most influential parameter contributing to the main cutting force and surface roughness, while cutting speed was identified as the dominant factor for tool life and depth of cut has minimal impact. Higher feed rates and cutting speeds increase tool wear due to greater heat and plastic deformation, but optimal surface quality can be achieved by combining high speeds with low feed rates and depths of cut. Recent reviews have identified a gap in studies specifically focusing on cutting speeds of 300–400 m/min with low feed rates (0.05–0.1 mm/rev), under both dry and MQL conditions, suggesting that this range is critical yet insufficiently explored (Rahman et al., 2024). Extending analysis to this speed regime addresses a key knowledge gap and could deliver important insights into the machinability of AISI 4340, supporting further optimization of tool performance and productivity in industrial applications.

Finite Element Analysis (FEA) is a numerical technique that solves complex problems by discretizing them into simpler, manageable elements, and subsequently synthesizing their responses to obtain an approximate solution (Soliman et al., 2020). FEA plays a critical role in machining research due to its capability to analyze intricate processes that are often difficult to capture experimentally. Researchers have employed FEA to address various specific machining challenges. Through simulation, FEA predicts machining outcomes, optimizes processing parameters, and forecasts tool life by evaluating cutting forces, temperatures, stresses, strains, and chip formation characteristics (Rahman et al., 2025). Additionally, FEA supports the optimization of tool geometry and performance by enabling virtual assessments of design alternatives, thereby improving tool life and machining efficiency (Wu et al., 2022). Importantly, FEA provides insights into scenarios that are experimentally challenging to replicate, though rigorous validation against empirical data remains essential to ensure the reliability and accuracy of simulation results. The method is also instrumental in investigating material behavior under conditions of high strain rates and elevated temperatures, contributing to the refinement of constitutive models like the Johnson-Cook model (Eltaggaz et al., 2020). To effectively handle the pronounced nonlinearities and large deformations characteristic of cutting processes, FEA software commonly incorporates adaptive remeshing techniques and explicit dynamic solvers.

Orthogonal cutting is a simplified machining model extensively used in engineering and research to explore the fundamentals of machining (Zetterberg, 2014). In orthogonal cutting, the tool's cutting edge is perpendicular to the cutting direction. This process involves relative motion between the tool and the workpiece, typically achieved through the cutting speed and feed rate. A thorough understanding of orthogonal cutting is essential for optimizing machining parameters, predicting cutting forces and temperature, and developing new cutting tools and strategies for advanced materials. In research, orthogonal cutting is often modelled as a 2D plane

strain problem, simplifying analysis and reducing model complexity. Plane strain condition is assumed which is valid as the workpiece's diameter is significantly larger than the uncut chip thickness (feed rate), leading to negligible strain in the width direction (Borsos et al., 2017; Ducobu et al., 2017; Qasim et al., 2015). Key factors influencing the cutting process include tool geometry, material properties, contact friction and cutting parameters (Konde, 2004).

Previous studies have emphasized the critical role of cutting parameters, particularly cutting speed and feed rate, in the machining of hardened AISI 4340 steels. Moreover, Finite Element Analysis (FEA) simulations have been widely recognized as instrumental tools for optimizing and analyzing machining processes. Nevertheless, there remains a notable gap in the investigation of AISI 4340 machinability at elevated cutting speeds ranging from 300 to 400 m/min combined with low feed rates. This study seeks to address this gap by employing ANSYS Explicit Dynamic FEA software to simulate high-speed machining conditions. The focus of the analysis is on evaluating cutting forces and cutting temperatures at the tool-chip interface. The findings provide valuable insights into the effects of hard turning on AISI 4340 steel within a relatively understudied high-speed machining regime and explore the potential for improving machinability.

2.0 EXPERIMENTAL PROCEDURE

2.1 Geometry and Boundary Conditions

A 2D orthogonal cutting model was developed in ANSYS Explicit Dynamic 2024 R2 to simulate the machining process of AISI 4340 steel using a carbide tool. The workpiece has dimensions of 5 mm in length and 0.5 mm in height. Meanwhile the cutting tool was designed with a rake angle of -6° and a clearance angle of 6° based on the actual geometry of AC4010K tool from Sumitomo. A sharp edge tool is a common simplification in FEA modelling taking into account the computational limitation due to larger contact area and extensively fine meshing requirement at the localized region (L. Wang et al., 2014; Wu et al., 2022). Tool edge radius also has minor influence once a steady state is reached in (Amrita Priyadarshini et al., 2012). Particularly at high speeds, the thermal load and wear rate are governed more by cutting speed as the dominant shear process which overshadows secondary geometric effects (Bakar et al., 2020; Li et al., 2018). Hence in the present study, a near sharp edge radius was modeled. This approach balances the need for geometric representation while maintaining a reasonable computational runtime.

Boundary conditions were applied by allowing the tool to move linearly in the cutting direction X-axis, while constraining the workpiece at the bottom and side edge. A zero-displacement condition at Y-axis is also applied at the tool side edge to avoid the tool from displacing out of the cutting axis. Cutting speed (V) is then applied as a velocity boundary condition to the tool, while the feed rate (f) is defined by the uncut chip thickness, representing the material removed per pass. For 2D analysis, plane strain assumption applied. Hence, the width is taken as a unit length which corresponds to the depth of cut. These methodologies and assumptions are well-supported by extensive research in the field (Borsos et al., 2017; Chen et al., 2022; Du et al., 2019; Eltaggaz et al., 2020; Juárez et al., 2019; Mabrouki & Rigal, 2006; Qian & Hossan, 2007). Figure 3 shows the geometry and boundary conditions of the 2D FEA model for cutting simulation.

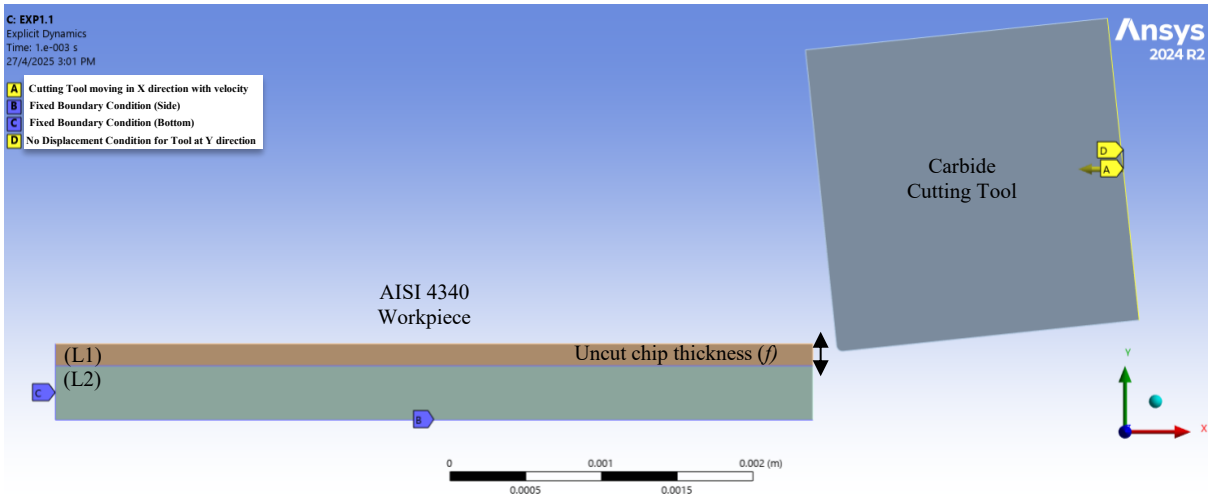

Figure 3. FEA model and boundary conditions for cutting simulation.

The workpiece and tool were meshed using linear element order within the Explicit Dynamic framework. The workpiece was discretized into two distinct layers: the upper layer (L1), representing the deformation zone, and the lower layer (L2), encompassing the remaining portion of the workpiece. To enhance data accuracy, a finer mesh was applied to the upper layer (L1) and the region surrounding the tool edge, supplemented further by adaptive meshing to accommodate the significant deformation and contact interactions occurring in this area. A mesh dependency study was performed by analyzing the cutting force and temperature outputs, which verified that simulation results remained stable with progressive mesh refinements and minimal difference of 5%. The final mesh configuration is illustrated in Figure 4, highlighting an extremely fine mesh in contact regions with minimum element size of 3 µm. The smallest time increment was set to 0.001s, corresponding to the lowest cutting speed employed for a single pass. Concentrating on the initial cutting pass provides fundamental insights into material and thermal behavior, chip morphology, and cutting forces, which are essential for understanding and optimizing the machining process. Additionally, single-pass simulations facilitate model validation against experimental data by delivering accurate predictions free from complexities associated with residual stresses and tool wear typically arising in multi-pass operations.

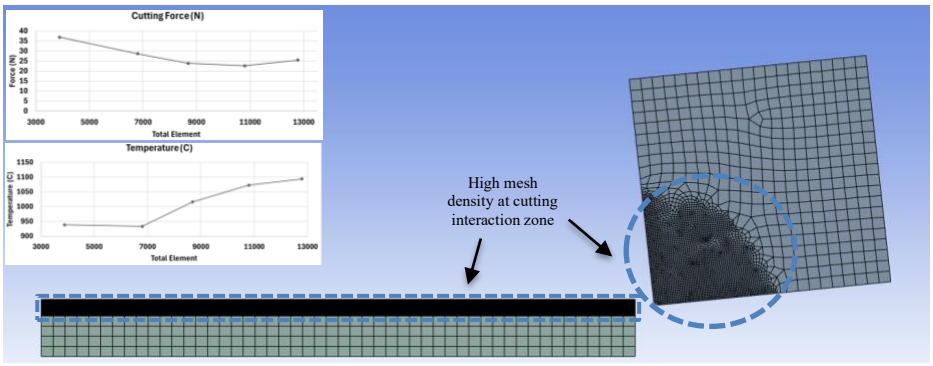

Figure 4. Mesh independent study and final mesh configuration.

2.2 Material Properties

Accurate definition of material properties is essential for producing reliable and meaningful outcomes in machining simulations. The workpiece is modeled as an elasto-plastic material to represent both elastic (recoverable) and plastic (permanent) deformations, which are critical for precise prediction of chip formation, cutting forces, temperatures, and stress distributions. The tool is often assumed to behave as a rigid body when the primary focus lies on the workpiece, owing to the tool's significantly higher hardness and stiffness, which render its deformation negligible and reduce computational demands (Methon et al., 2024). However, when force and thermal effect are of interest, modeling the tool as a deformable body becomes necessary. This approach, although computationally more intensive, allows the simulation of recoverable tool deformation under load and more accurately captures tool behavior, particularly at elevated cutting speeds (Ghani et al., 2024; Salvatore et al., 2013). To balance computational efficiency and accuracy, a rigid constraint is imposed along the cutting direction while still simulating thermal effects effectively.

Table 1 summarizes the physical properties of AISI 4340 steels and the coated carbide tool utilized in this study based on previous research on the same material. For simplification, the coated carbide tool is assigned combined material properties: thermal properties are based on the alumina (Al_2O_3) coating layer, while the remaining mechanical and physical properties correspond to the carbide substrate, following the tool supplier's recommendations (Sumitomo Electric Group, 2023).

Table 1: Physical properties of workpiece and cutting tool (Iynen et al., 2021; Mabrouki & Rigal, 2006; Özel & Zeren, 2007).

Properties	Workpiece (AISI 4340)	Coated carbide tool (AC4010K)
Thermal Conductivity, k (W/m^{o}C)	44.5	30
Density ρ (kg/m^3)	7850	15000
Young's Modulus, E (GPa)	205	800
Poisson's ratio ν	0.3	0.2
Specific heat, C_p (J/kg/^{o}C)	475	800
Expansion coefficient, α (10^{-5})	1.37	-

The choice of constitutive models, damage criteria, and material constants significantly influences the predicted chip morphology, cutting forces, tool wear, and surface integrity. The Johnson-Cook (JC) constitutive model is largely used to characterize the workpiece material under the high strain rates and temperatures typical of high-speed machining, accounting for three main material characteristics that influence its machinability: strain hardening, strain-rate sensitivity, and thermal softening (Borsos et al., 2017; Iynen et al., 2021; Soliman et al., 2020). Equation (1) shows the plastic flow stress formula using Johnson-Cook constitutive model.

$$\sigma = [A + B(\varepsilon^n)]\left[1 + C\ln\left(\frac{\dot{\varepsilon}}{\dot{\varepsilon}_0}\right)\right]\left[1 - \left(\frac{T - T_r}{T_m - T_r}\right)^m\right] \quad (1)$$

Where σ is the material flow stress, A is the yield strength, B is the hardening modulus, C is the strain rate factor, ε is the plastic strain, $\dot{\varepsilon}$ is the strain rate, $\dot{\varepsilon}_0$ is the reference strain rate given

as 1s-1, T is the temperature of the material, T_m is the melting point of the material, T_r is the room temperature, n is the work hardening coefficient and m is the thermal softening coefficient.

In machining processes, both surface integrity and hardness are impacted by high strain rates and rapid chip formation. Therefore, it is crucial to incorporate strain hardening into the material model. Strain rate sensitivity adjusts the material's stress-strain relationship under varying feed rates and cutting speeds. Additionally, thermal softening accounts for material softening due to high machining temperatures, which can reach up to 1500°C during AISI 4340 deformation. Table 2 shows the JC material constants used for AISI 4340 plastic input which has been used for material hardness up to 48HRC based on previous studies (Jiang & Wang, 2019; Johnson & Cook, 1983; Mabrouki & Rigal, 2006).

Table 2: JC material constants for AISI 4340 steel.

Material	A **[MPa]**	B **[MPa]**	n	C	m	T_m(℃)	T_r(℃)
AISI 4340	792	510	0.26	0.014	1.02	1520	20

Additionally, simulating chip separation necessitates the inclusion of failure models, with the JC damage model being commonly employed to predict material failure based on strain, strain rate, and temperature. The model used for ductile material consists of two phases, a damage initiation and a damage evolution phase. Equation (2) shows the equivalent strain at fracture $\bar{\varepsilon}_f{}^{pl}$ based on the JC model (Johnson & Cook, 1985; Sulaiman et al., 2013).

$$\bar{\varepsilon}_f{}^{pl} = \left[d_1 + d_2 \exp\left(d_3 \frac{p}{q}\right)\right]\left[1 + d_4 \ln\left(\frac{\varepsilon^{pl}}{\dot{\varepsilon}_0}\right)\right]\left[1 + d_5 \frac{T - T_r}{T_{m-T_r}}\right] \qquad (2)$$

Where d_1 - d_5 are damage coefficients and $\frac{p}{q}$ is the ratio of pressure and Von Mises stress. The fraction damage or fracture is initiated in an element when the damage parameter D reached unity 1 or exceeded it. The damage parameter used in the simulation is given as Equation (3):

$$D = \sum\left(\frac{\Delta\bar{\varepsilon}^{pl}}{\bar{\varepsilon}_f{}^{pl}}\right) \qquad (3)$$

Where $\Delta\bar{\varepsilon}^{pl}$ is the increment of equivalent plastic strain and $\bar{\varepsilon}_f{}^{pl}$ is equivalent strain at fracture. According to the damage model law, the equivalent plastic strain $\Delta\bar{\varepsilon}^{pl}$ response is updated at each of the simulation increments. Table 3 shows the damage coefficients used in the model for AISI 4340 steel.

Table 3: JC damage coefficients for AISI 4340 steel.

Initial failure strain, d_1	**Exponential factor,** d_2	**Triaxiality factor,** d_3	**Strain rate factor,** d_4	**Temperature factor,** d_5
0.05	3.44	-2.12	0.002	0.61

For the tool-workpiece interaction, a connection is defined using body interactions with penalty formulation and frictional definition based on the Coulomb friction model (Chen et al., 2022). The cutting tool's surface is defined as the main body, while the workpiece's surface acts

as the secondary body in the contact definition. The model in its simple form is defined as Equation (4):

$$\tau = \mu\sigma_n \quad (4)$$

Here τ is the frictional shear stress, μ is the friction coefficient and σ_n is the normal stress. In this study, friction coefficient of 0.3 is applied based on the relevant literature for hardened steel under high speed regime (Natasha et al., 2016).

2.3 Design of Experiment (DOE)

Table 4 provides a detailed summary of the experimental design (DOE) to be implemented in this study. The design includes three different levels of simulation, varying by cutting speed, feed rate, and depth of cut. The cutting parameters are selected based on the previous gap findings for AISI 4340 steel (Rahman et al., 2024). The Taguchi L9 orthogonal array method has been applied to the factors and levels to conduct all 9 simulations labeled as Trial 1 – 9 as presented in Table 5.

Table 4: Factors and level used in the simulation.

Factor / Level	1	2	3
Cutting Speed (m/min)	300	350	400
Feed rate (mm/rev)	0.05	0.075	0.1
Depth of cut (mm)	0.1	0.2	0.3

Table 5: Design of Experiment (DOE) list based on Taguchi L9.

Trial	Cutting Speed (m/min)	Feed Rate (mm/rev)	Depth of Cut (mm)
1	300	0.050	0.1
2	300	0.075	0.2
3	300	0.100	0.3
4	350	0.050	0.2
5	350	0.075	0.3
6	350	0.100	0.1
7	400	0.050	0.3
8	400	0.075	0.1
9	400	0.100	0.2

In high-speed machining (HSM), the interrelationship between cutting force and cutting temperature is fundamental to understanding material behavior and tool performance, as these factors form a complex, interactive system. Comprehensive understanding of this interrelationship is essential for accurately predicting and controlling the cutting forces and temperature, ultimately enabling better control of tool wear and the optimization of tool life. The results section will further elaborate on their evolution in response to the applied parameters as listed in the DOE. To ensure model reliability, relation with experimental data is also discussed.

3.0 RESULTS AND DISCUSSION

3.1 Cutting Force

Table 6 summarizes the cutting forces recorded for Trial 1 through 9. These forces were extracted from the tool edge nodes and computed as resultant forces representing the total cutting force (Soliman et al., 2020). These forces were initially obtained on a per-unit-width basis (N/mm) under the 2D plane strain assumption and subsequently scaled by the depth of cut applied to reflect the actual cutting conditions.

Table 6: Cutting force data from simulation.

Trial	Cutting Speed (m/min)	Feed Rate (mm/rev)	Depth of Cut (mm)	Resultant Cutting Force (N)
1	300	0.050	0.1	21.34
2	300	0.075	0.2	43.67
3	300	0.100	0.3	76.86
4	350	0.050	0.2	42.69
5	350	0.075	0.3	68.87
6	350	0.100	0.1	25.83
7	400	0.050	0.3	70.82
8	400	0.075	0.1	20.84
9	400	0.100	0.2	49.58

Based on the data presented in Table 6, a clear correlation between cutting parameters and cutting force is evident. From Trial 1 to Trial 3, where the feed rate and depth of cut increase while maintaining a constant cutting speed of 300 m/min, the cutting force correspondingly rises from 21.34 N to 76.86 N. This trend aligns with expectations, as higher feed rates result in increased uncut chip thickness and material removal volume, thereby elevating the cutting forces (Qasim et al., 2015). Likewise, an increase in the depth of cut expands the cross-sectional area of the undeformed chip, which in turn leads to greater cutting force requirements (Ghani et al., 2024; Zhang et al., 2021). Extending further the analysis from Trial 1 to Trial 9, a different pattern emerges. As the cutting speed increases from 300 m/min to 400 m/min, the cutting force exhibits fluctuations rather than a linear trend. This behavior is partly attributed by the variations in the depth of cut, which do not increase proportionally with the feed rate. For instance, an increase in cutting speed from 300 m/min (Trial 3) to 400 m/min (Trial 9), while maintaining a constant feed rate but with reduced depth of cut led to a decrease in cutting force from a maximum of 76.86 N to 49.58 N.

Additionally, increasing the cutting speed is shown to further reduce the cutting force. The highest parameter setting (Trial 9), which corresponds to the maximum cutting speed, yields a lower cutting force compared to most other experiments. Notably, the lowest cutting force is observed at 400 m/min in Trial 8. Despite the application of a larger feed rate, increasing the cutting speed from 300 m/min (Trial 1) to 400 m/min (Trial 8) results in a slight force reduction from 21.34 N to 20.84 N. This modest decrease suggests a thermal softening effect at elevated speeds that mitigates the load increase associated with higher material removal rates. This observation aligns with the well-established understanding that higher cutting speeds reduce cutting forces due to thermal softening of the workpiece material, which consequently lowers its shear strength (Konde, 2004). Furthermore, it substantiates the maximum cutting force recorded

in Trial 3, where the lowest cutting speed was combined with the highest feed rate and depth of cut.

A comparative analysis was conducted with a recent experimental study by Saima et al (Jouini et al., 2025), which employed a turning process on hardened AISI 4340 steel circa 50 HRC under the same high-speed machining regime. Figure 5 presents a comparison of cutting forces between the experimental results and the current FEA simulations, using identical parameter settings for all experiments. It is important to note that the experimental data report only the main cutting force component, measured during the initial pass using an in-house dynamometer. Accordingly, the cutting force component along the cutting direction (X-axis) was extracted from the simulation results for a lateral comparison.

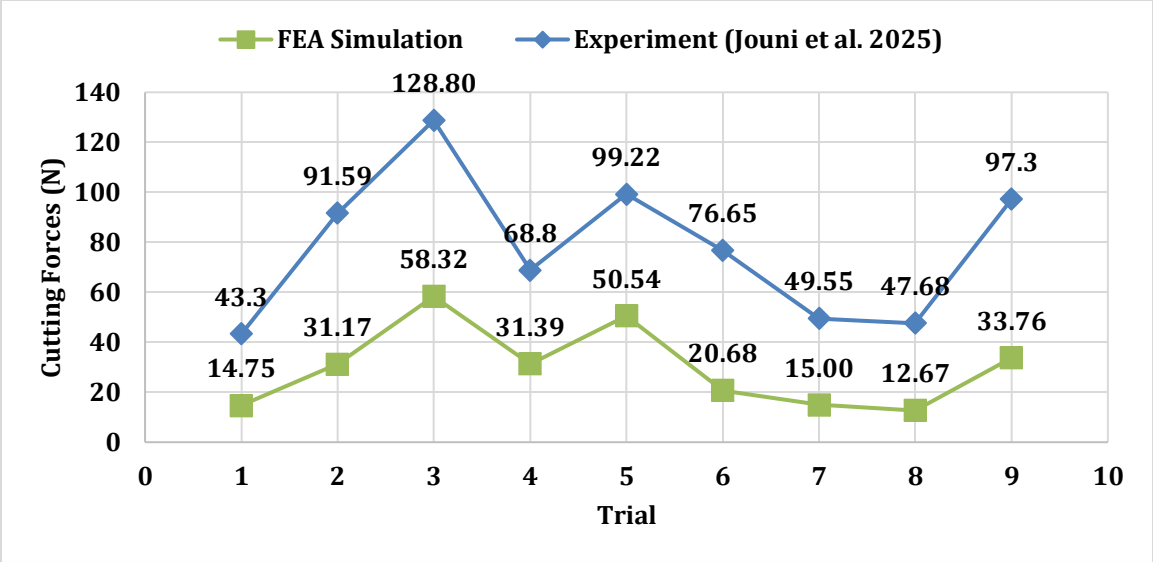

Figure 5: Cutting force data trend between FEA simulation and previous experimental study by (Jouini et al., 2025).

The study reveals a generally consistent trend between the experimental results and simulation outcomes. Under a constant cutting speed, cutting forces initially increase, reaching a maximum at Trial 3, before decreasing and exhibiting fluctuations through to Trial 6 as the cutting speed increases further. This behavior confirms the non-linear trend observed in the simulation, where the interplay of cutting speed, feed rate, and depth of cut collectively influences the cutting force.

Despite the similarity in trends, an average discrepancy of approximately 60% in force magnitude is noted between the experimental and simulated values. This disparity primarily arises from differences in the tool edge radius employed. Although the cutting parameters and workpiece and tool materials are comparable, the simulation utilizes a near sharp edge radius (0.04 mm) compared to the experimental tool (0.4 mm), resulting in lower cutting forces. The reduced contact area at the tool-workpiece interface decreases material ploughing and deformation, thereby lowering cutting resistance and force relative to the experiment with a larger edge radius (B. Wang & Liu, 2014). Supporting this, (Trent & Wright, 2000) report that a reduction in contact area at the tool-chip interface can yield between 50% to 80% decrease in

cutting forces. Additionally, an experimental comparison between a sharper edge radius (0.06 mm) and a worn, blunted edge tool (0.3 mm) demonstrated more than a 100% increase in tangential cutting force, highlighting the significant impact of edge geometry on cutting performance (Wagri et al., 2023).

A sensitivity analysis incorporating the actual tool radius was performed, resulting in a reduction of the force discrepancy to below 20%. However, chip separation which is a critical factor for accurately studying temperature at the tool-chip interface was not observed. This absence is attributed to the dominant ploughing effect arising from a large edge radius relative to the uncut chip thickness, coupled with the requirement for an extremely fine mesh in the cutting zone, which is computationally not effective. Nonetheless, given the consistent trends in cutting forces observed between experimental results and simulations under identical cutting conditions, the simplification of the tool edge geometry in the model is justified.

3.2 Cutting Temperature

High-speed machining is a thermally coupled process where elevated temperatures significantly influence material behaviour and cutting mechanics. Thermal softening of the workpiece reduces its flow stress and resistance to deformation, leading to decreased cutting forces (EMİR, 2024). Increasing cutting speed and feed rate further elevate thermal loads due to increased friction, diffusion, and oxidation which accelerates tool wear. Interestingly, reduced cutting forces at high temperature may also lower tool stresses and wear, as the softened workpiece causes less abrasive damage (Hadad & Ebrahimi, 2023). Controlling temperature at the cutting zone is thus critical for optimizing tool life in HSM.

The FEA model enables prediction of peak temperature at the tool-chip interface nodes and supports more effective localization of heat sources, which is critical for future heat mitigation strategies. Figure 6 shows the temperature distribution profile at the critical zones where high heat is generated during machining for both the lowest speed settings (Trial 1) and the highest speed settings (Trial 9) for comparison. To ensure consistency for different speed and time step, the profile is taken during mid pass for each case where the chip is continuously formed and at an interface with the tool.

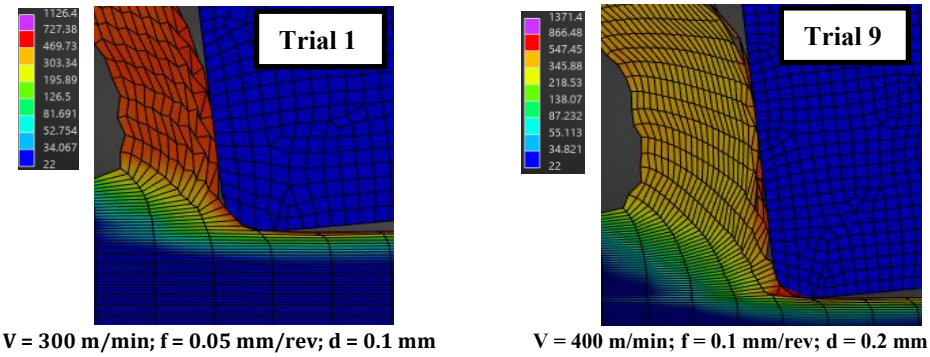

Figure 6: Temperature contour at the cutting zone for Trial 1 for lowest speed and Trial 9 for highest speed.

Based on Figure 6, continuous chip formation is observed in both experiments, which is characteristic of high cutting speeds due to the substantial plastic deformation and elevated

temperatures generated within the deformation zones. The peak tool-chip interface temperature for Trial 1 is recorded at 727.34°C as a result of intense material shearing, thermal softening and friction at the interfaces. Meanwhile, Trial 9 exhibits a substantial 17.5% increase in maximum temperature attributable to the combined effects of higher cutting speed and feed rate. The temperature spread in the chip section is also at the higher spectrum for Exp 9 at between 345.88°C - 727.34°C, in comparison to 303.33°C to 727.34°C for Trial 1. According to previous study (Demirpolat et al., 2023), increased cutting speed elevates the deformation rate and friction at the tool-chip interface, thereby converting more mechanical energy into thermal energy per unit time, and consequently raising the temperature. Trial 9 also produces thicker chips because of the higher feed rate compared to Trial 1.

In contrast, the temperature within the tool region remains relatively low, owing to the thermal insulating properties of the Al_2O_3 coating, which protects the carbide tool substrate from excessive heat and minimal heat dissipation during initial cutting pass. This behavior is expected in high-speed regime at initial condition where contact interaction is short. However, with continous cutting, the coating layer in actual operations will progressively wear away, exposing the carbide substrate. This will result in increased temperature exposure to the tool, potentially compromising tool rigidity and reducing tool life. Therefore, monitoring and mitigating temperature at the tool-chip interface particularly in the initial stage is critical for assessing tool durability. Table 7 presents the maximum temperatures measured at the tool-chip interface for all 9 trials.

Table 7: Cutting temperature data from simulation.

Trial	Cutting Speed (m/min)	Feed Rate (mm/rev)	Depth of Cut (mm)	Maximum Temperature at Interface (°C)
1	300	0.050	0.1	727.34
2	300	0.075	0.2	771.39
3	300	0.100	0.3	713.51
4	350	0.050	0.2	666.57
5	350	0.075	0.3	756.41
6	350	0.100	0.1	800.74
7	400	0.050	0.3	825.17
8	400	0.075	0.1	781.23
9	400	0.100	0.2	866.48

Based on the data presented in Table 7, it is evident that the cutting temperature generally increases with the rise in cutting speed from 300 m/min to 400 m/min. The highest recorded temperature occurs in Trial 9, reaching 866.48 °C, which is approximately 26% greater than the lowest temperature found in Trial 4 at 666.57 °C. This temperature fall within the typical range reported in previous studies on high-speed machining of AISI 4340 steel and similar high-strength steels. Specifically, literature indicates that temperatures at the tool-chip interface can approach between 600°C to 1000 °C, while the cutting edge temperature typically remains lower (Abukhshim et al., 2006; Trent & Wright, 2000). This consistency supports the reliability of the simulation results within the expected thermal regime for such machining operations. It is also noteworthy that for a fixed cutting speed, the cutting temperature exhibits fluctuations with increasing feed rate; however, an overall increasing trend is observed as the feed rate increases

from 0.05 mm/rev to 0.1 mm/rev. This behavior suggests that while cutting speed predominantly drives temperature elevation due to increased strain rates and frictional heating, the feed rate also modulates the thermal response, likely through its effect on material removal rate and tool-chip contact conditions.

Comparing these thermal data to cutting force measurements reported in Table 6, no straightforward correlation emerges. For instance, the lowest cutting forces at Trial 8 did not correspond to the highest temperature expected due to thermal softening although it is at the higher spectrum. Conversely, the largest cutting force at Trial 3 also does not mirror lowest temperature. Such observations imply that cutting speed primarily governs temperature generation, while feed rate and depth of cut exert a more pronounced influence on cutting forces. This observations aligns with the findings of statistical analyses using Signal-to-Noise (S/N) ratio and Analysis of Variance (ANOVA) conducted by (Jouini et al., 2025), which identified feed rate as the most significant parameter influencing cutting force, whereas cutting speed was the dominant factor affecting tool life. The relationship between cutting temperature and tool life is further shown in Figure 7, where simulated temperature data are compared with experimentally determined tool life, highlighting the critical role of thermal effects in tool integrity.

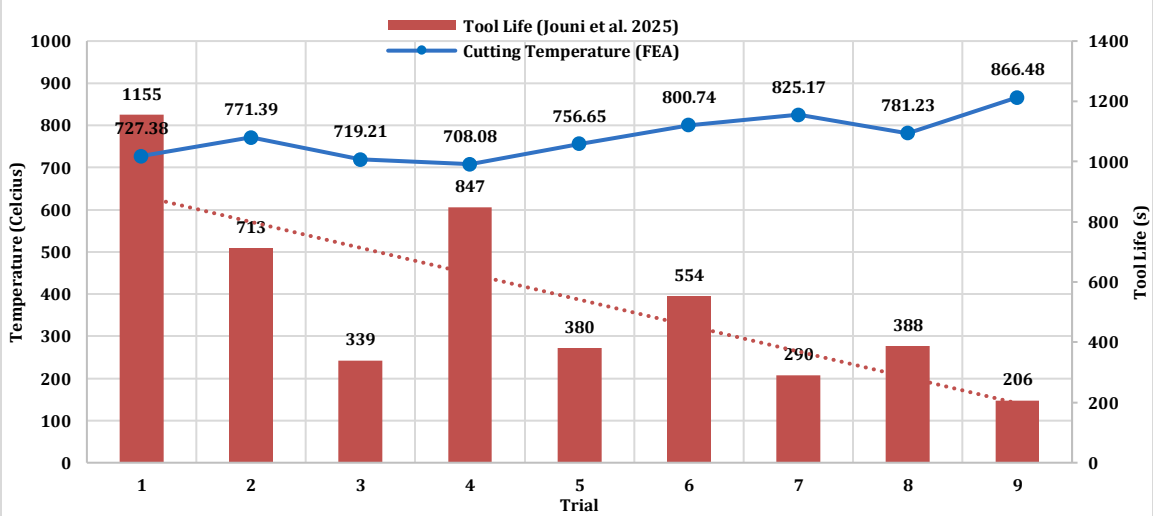

Figure 7: Cutting temperature data from FEA simulation and relation to to tool life obtained from experimental study by (Jouini et al., 2025).

Based on Figure 7, the relationship between tool-chip interface temperature and tool life across all experiments reveals an inverse trend, whereby increasing cutting temperature corresponds with decreasing tool life. In general, the data show that as the speed increases across the experiment, temperature rises, and tool life diminishes substantially. For instance, Trial 1 records a tool life close to 1155 seconds (19.3 minutes) at a lower temperature (727.34°C), whereas Trial 9 exhibits the highest temperature (866.48°C) alongside the shortest tool life of approximately 206 seconds (3.4 minutes). This clear pattern underscores the detrimental impact of elevated temperatures on tool durability that promote wear mechanisms such as thermal softening, diffusion, and adhesive wear, thereby accelerating tool degradation. This supports the previous statement in which as the machining progress, the tool's coating layer has become

ineffective in combating the high temperature at the interface resulting in the rapid wear and shorter life.

Variations in feed rates introduce additional thermal and mechanical loading fluctuations that affect both temperature and tool life. Notably, although Trial 4 recorded the lowest temperature, the longest tool life was observed in Trial 1, likely due to a combination of lower cutting forces and cutting speed as shown in Table 6 and Figure 5, highlighting the interplay of other factors beyond temperature alone. The presented data consolidates the understanding that while cutting temperature is a critical determinant of tool life, an integrated approach considering all cutting parameters is necessary to enhance tool performance and longevity. However, as speed progress further, the influence of temperature becomes more critical for the tool life.

3.3 Taguchi Analysis

To gain a deeper understanding of the influence of cutting parameters on the machining response, response table for signal-to-noise (S/N) ratio, main effect plots and Analysis of Variance (ANOVA) from Taguchi analysis is presented in Table 8, Figure 8 and Table 9 respectively for cutting force. The same analysis is discussed for cutting temperature and presented in Table 10, Figure 9 and Table 11 respectively. In this analysis, *V* denotes the cutting speed, *f* represents the feed rate, and *d* indicates the depth of cut.

Table 8: Response Table for SN Ratios (Smaller is better) for cutting force.

Level	**V**	**f**	**d**
1	-32.37	-28.81	-27.07
2	-32.54	-31.98	-33.11
3	-29.17	-33.29	-33.9
Delta	3.36	4.48	6.83
Rank	**3**	**2**	**1**

Table 9: ANOVA for cutting force.

Parameters	**DF Value**	**Seq SS**	**Adj SS**	**Adj MS**	**F-Value**	**P-Value**	**Contribution**
V	2	477.9	477.9	238.9	0.95	0.513	**13.69%**
f	2	751.3	751.3	375.6	1.49	0.401	**21.51%**
d	2	1759.4	1759.4	879.7	3.5	0.222	**50.38%**
Residual	2	503.4	503.4	251.7			
Total	8	3491.8					

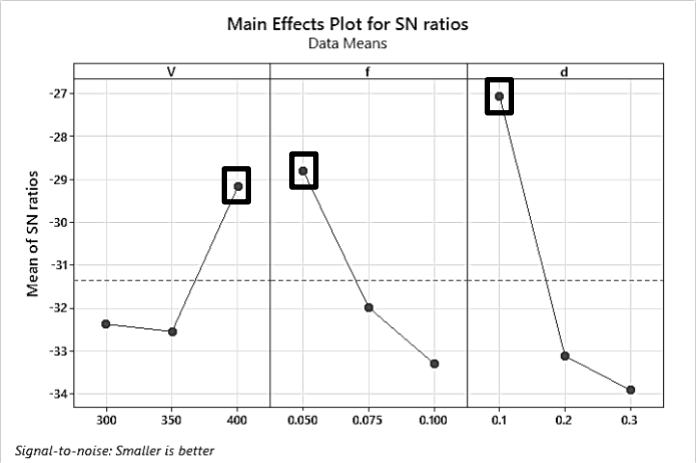

Figure 8: Main effect plots for cutting force. Boxed point is the optimum parameter.

Table 10: Response Table for SN Ratios (Smaller is better) for cutting temperature.

Level	**V**	**f**	**d**
1	-52.67	-52.8	-52.97
2	-52.83	-52.98	-53.08
3	-53.5	-53.21	-52.94
Delta	0.83	0.41	0.13
Rank	**1**	**2**	**3**

Table 11: ANOVA for cutting temperature.

Parameters	**DF Value**	**Seq SS**	**Adj SS**	**Adj MS**	**F-Value**	**P-Value**	**Contribution**
V	2	3155.44	3155.44	1577.72	1.89	0.346	**56.26%**
f	2	689.84	689.84	344.92	0.41	0.707	**12.30%**
d	2	96.01	96.01	48.01	0.06	0.946	**1.71%**
Residual	2	1667.52	1667.52	833.76			
Total	8	5608.82					

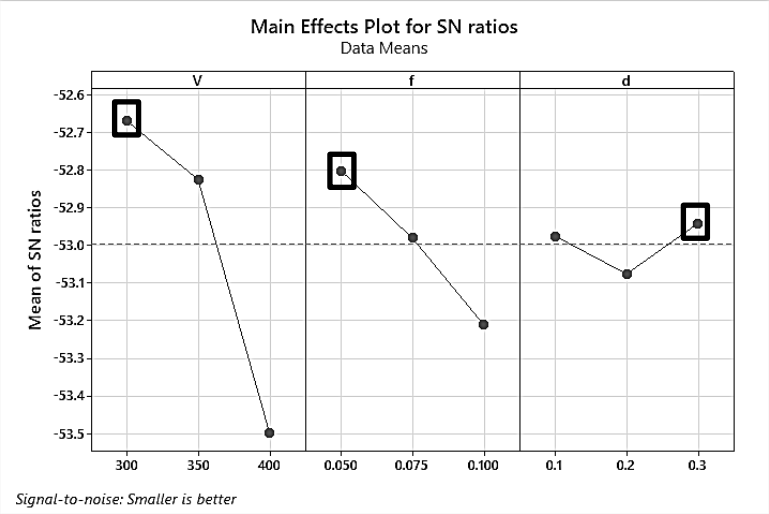

Figure 9: Main effect plots for cutting temperature. Boxed point is the optimum parameter.

Based on the trends observed from Taguchi analysis, distinct differences emerge between the effects of cutting parameters on cutting force and cutting temperature. As shown in Table 8 and 9 for cutting forces, the depth of cut (d) has the most significant influence on cutting force, followed by feed rate and, to a lesser extent, cutting speed based on ranking and percentage contribution. According to the "smaller-is-better" criterion, the optimal combination for minimizing cutting force is a cutting speed of 400 m/min, feed rate of 0.05 mm/rev and depth of cut of 0.1 mm as shown in Figure 8. In contrast, Table 10 and 11 for cutting temperature indicates that cutting speed has the greatest influence on cutting temperature, followed by feed rate and depth of cut based on ranking and percentage contribution. Applying the same "smaller-is-better" criterion, the optimal combination for lowest cutting temperature is achieved at a cutting speed of 300 m/min, feed rate of 0.05 mm/rev, and depth of cut of 0.3 mm. These observed trends are also consistent with the findings discussed in the previous section regarding cutting force and temperature change.

CONCLUSIONS

Despite extensive research on the machinability of AISI 4340 steel, there remains a notable gap in investigations focusing on cutting speeds within the 300–400 m/min range combined with lower feed rates in supporting further optimization of tool performance and productivity of this material in industrial applications. This study addresses this gap by systematically analyzing cutting forces and tool-chip interface temperatures under high-speed machining conditions through finite element analysis (FEA) simulation. The results demonstrate that cutting speed is the predominant factor influencing cutting temperature, whereas depth of cut exerts a greater effect on cutting forces. A strong correlation between simulation outcomes and experimental data was observed, validating the reliability of the developed model. As cutting speed increases, tool-chip interface temperatures rise correspondingly, while cutting forces peak at the highest feed rates and depths of cut, collectively impacting tool life.

This research provides valuable insights into the hard turning process of AISI 4340 steel, offering potential pathways for improving machinability and productivity particularly tool performance optimization under dry machining conditions within this relatively underexplored high-speed regime. The FEA model effectively predicts peak temperatures at tool-chip interface nodes, enabling more precise localization of heat generation zones, which is critical for the development of targeted cooling or lubrication strategies. Future work could incorporate sustainable cooling methods such as minimum quantity lubrication (MQL), employing integrated FEA and computational fluid dynamics (CFD) simulations to assess coolant effects on interface temperature distribution. Additionally, detailed investigations into tool wear mechanisms will further consolidate understanding of tool degradation and life trends, enhancing correlation with simulation predictions and informing more robust machining strategies for better productivity.

ACKNOWLEDGEMENT

The authors thankfully acknowledged the financial support provided by Ministry of Higher Education Malaysia under FRGS/1/2024/TK10/UKM/01/1 grant.

REFERENCES

Abukhshim, N. A., Mativenga, P. T., & Sheikh, M. A. (2006). Heat generation and temperature prediction in metal cutting: A review and implications for high speed machining. International Journal of Machine Tools and Manufacture, 46(7–8), 782–800. https://doi.org/10.1016/j.ijmachtools.2005.07.024

Ahmad, A. A., Ghani, J. A., & Che Haron, C. H. (2022). Effect of cutting parameters on tool life during end milling of AISI 4340 under MQL condition. Industrial Lubrication and Tribology, 74(4), 392–401. https://doi.org/10.1108/ILT-08-2021-0295

Ahmad, A. A., Ghani, J. A., & Haron, C. H. C. (2021). Green lubrication technique for sustainable machining of AISI 4340 alloy steel. Jurnal Tribologi, 28(October 2020), 1–19.

Ahmad, A. A., Ghani, J. A., & Haron, C. H. C. (2022). Potential of Bio-Metal Cutting Fluid from Treated Recycled Cooking Oil for Metal Cutting Fluid Application. Journal of Mechanical Engineering, 19(1), 83–97.

Al-Ghamdi, K. A., & Iqbal, A. (2015). A sustainability comparison between conventional and high-speed machining. Journal of Cleaner Production, 108, 192–206. https://doi.org/10.1016/j.jclepro.2015.05.132

Amrita Priyadarshini, Surjya K Pal, & Arun K Samantaray. (2012). Influence of the Johnson Cook material model parameters and friction models on simulation of orthogonal cutting process. Journal of Machining and Forming Technologies, 4(1/2), 59–83.

Azaath, L. M., Mohan, E., & Natarajan, U. (2020). Effect of rake angle and tool geometry during machining process of AISI 4340 steel in finite element approach. Materials Today: Proceedings, 37(Part 2), 3731–3736. https://doi.org/10.1016/j.matpr.2020.10.196

Bag, R., Panda, A., Sahoo, A. K., & Kumar, R. (2020). A Comprehensive Review on AISI 4340 Hardened Steel: Emphasis on Industry Implemented Machining Settings, Implications, and Statistical Analysis. International Journal of Integrated Engineering, 12(8), 61–82. https://doi.org/10.30880/ijie.2020.12.08.007

Bag, R., Panda, A., Sahoo, A. K., & Kumar, R. (2022). Sustainable High-Speed Hard Machining of AISI 4340 Steel Under Dry. Arabian Journal for Science and Engineering. https://doi.org/10.1007/s13369-022-07094-9

Bakar, H. N. A., Ghani, J. A., & Che Haron, C. H. (2020). Influence of rounded cutting-edge radius and machining parameters on surface roughness and tool wear in milling AISI H13 steel under dry and cryogenic machining. Jurnal Tribologi, 24(February), 52–64.

Borsos, B., Csörgo, A., Hidas, A., Kotnyek, B., Szabó, A., Kossa, A., & Stépán, G. (2017). Two-dimensional finite element analysis of turning processes. Periodica Polytechnica Mechanical Engineering, 61(1), 44–54. https://doi.org/10.3311/PPme.9283

Chen, G., Caudill, J., Ren, C., & Jawahir, I. S. (2022). Numerical modeling of Ti-6Al-4V alloy orthogonal cutting considering microstructure dependent work hardening and energy density-based failure behaviors. Journal of Manufacturing Processes, 82(August), 750–764. https://doi.org/10.1016/j.jmapro.2022.08.032

Chinchanikar, S., & Choudhury, S. K. (2014). Evaluation of Chip-tool Interface Temperature: Effect of Tool Coating and Cutting Parameters during Turning Hardened AISI 4340 Steel. Procedia Materials Science, 6(Icmpc), 996–1005. https://doi.org/10.1016/j.mspro.2014.07.170

da Silva, L. R., Couto, D. A., dos Santo, F. V., Duarte, F. J., Mazzaro, R. S., & Veloso, G. V. (2020). Evaluation of machined surface of the hardened AISI 4340 steel through roughness and residual stress parameters in turning and grinding. International Journal of Advanced Manufacturing Technology, 107(1–2), 791–803. https://doi.org/10.1007/s00170-020-05046-x

Das, S. R., Kumar, A., Dhupal, D., & Mohapatra, S. K. (2013). Optimization of Surface Roughness in Hard Turning of AISI 4340 Steel using Coated Carbide Inserts. International Journal of Information and Computation Technology, 3(9), 871–880. http://www.irphouse.com/ijict.htm

Demirpolat, H., Binali, R., Patange, A. D., Pardeshi, S. S., & Gnanasekaran, S. (2023). Comparison of Tool Wear, Surface Roughness, Cutting Forces, Tool Tip Temperature, and Chip Shape during Sustainable Turning of Bearing Steel. Materials, 16(12), 4408. https://doi.org/10.3390/ma16124408

Du, M., Cheng, Z., & Wang, S. (2019). Finite element modeling of friction at the tool-chip-workpiece interface in high speed machining of Ti6Al4V. International Journal of Mechanical Sciences, 163(March), 105100. https://doi.org/10.1016/j.ijmecsci.2019.105100

Ducobu, F., Rivière-Lorphèvre, E., & Filippi, E. (2017). Finite element modelling of 3D orthogonal cutting experimental tests with the Coupled Eulerian-Lagrangian (CEL) formulation. Finite Elements in Analysis and Design, 134(May), 27–40. https://doi.org/10.1016/j.finel.2017.05.010

Eltaggaz, A., Said, Z., & Deiab, I. (2020). An integrated numerical study for using minimum quantity lubrication (MQL) when machining austempered ductile iron (ADI). International Journal on Interactive Design and Manufacturing, 14(3), 747–758. https://doi.org/10.1007/s12008-020-00662-z

EMİR, E. (2024). Experimental investigation and FEM analysis of chip morphology in the turning of ASTM F-75 CoCrMo alloy. Sigma Journal of Engineering and Natural Sciences – Sigma Mühendislik ve Fen Bilimleri Dergisi, 42(3), 679–691. https://doi.org/10.14744/sigma.2023.00130

Ghani, J. A., Ismanizan, M. A., Rahman, H. A., Haron, C. H. C., Juri, A. Z., Kasim, M. S., & Rizal, M. (2024). Machining analysis of S45C carbon steel using finite element method. Jurnal Tribologi, 40(August 2023), 226–246.

Guo, Y. B., & Yen, D. W. (2004). A FEM study on mechanisms of discontinuous chip formation in hard machining. Journal of Materials Processing Technology, 155–156(1–3), 1350–1356. https://doi.org/10.1016/j.jmatprotec.2004.04.210

Hadad, M., & Ebrahimi, S. M. (2023). Towards Industry 4.0 and Sustainable Manufacturing Applying Environmentally Friendly Machining of a Precipitation Hardened Stainless Steel Using Hot Turning Process. Applied Sciences (Switzerland), 13(22). https://doi.org/10.3390/app132212405

Iynen, O., Ekşi, A. K., Özdemir, M., & Akylldlz, H. K. (2021). Experimental and numerical investigation of cutting forces during turning of cylindrical AISI 4340 steel specimens. Materialpruefung/Materials Testing, 63(5), 402–410. https://doi.org/10.1515/mt-2020-0069

Jiang, L., & Wang, D. (2019). Finite-element-analysis of the effect of different wiper tool edge geometries during the hard turning of AISI 4340 steel. Simulation Modelling Practice and Theory, 94(March), 250–263. https://doi.org/10.1016/j.simpat.2019.03.006

Johnson, G. R., & Cook, W. H. (1983). A Computational Constitutive Model and Data for Metals Subjected to Large Strain, High Strain Rates and High Pressures. The Seventh International Symposium on Ballistics, 541–547.

Johnson, G. R., & Cook, W. H. (1985). Fracture characteristics of three metals subjected to various strains, strain rates, temperatures and pressures. Engineering Fracture Mechanics, 21(1), 31–48. https://doi.org/10.1016/0013-7944(85)90052-9

Jouini, N., A. Ghani, J., Yaqoob, S., & Juri, A. Z. (2025). Optimized Machining Parameters for High-Speed Turning Process: A Comparative Study of Dry and Cryo+MQL Techniques. Processes, 13(3), 1–18. https://doi.org/10.3390/pr13030739

Juárez, M. A. P., Gómez, E. A., Mora, H. P., Orozco, E. L., Arredondo, J. F. R., & Silva, M. L. C. (2019). Finite element simulation and experimental analysis of cutting forces in orthogonal turning in AISI-1045 steel. Computacion y Sistemas, 23(1), 7–20. https://doi.org/10.13053/CyS-23-1-3134

Konde, P. (2004). FINITE ELEMENT ANALYSIS OF SHEAR-LOCALIZATION IN HIGH-SPEED MACHINING OF AISI 4340 STEEL. Oklahoma State University.

Li, B., Zhang, S., Yan, Z., & Jiang, D. (2018). Influence of edge hone radius on cutting forces , surface integrity , and surface oxidation in hard milling of AISI H13 steel. 1153–1164.

Mabrouki, T., & Rigal, J. F. (2006). A contribution to a qualitative understanding of thermo-mechanical effects during chip formation in hard turning. Journal of Materials Processing Technology, 176(1–3), 214–221. https://doi.org/10.1016/j.jmatprotec.2006.03.159

Methon, G., Courbon, C., Espinoux, F., Frelechoux, R., & Rech, J. (2024). A numerical approach to investigate the influence of cutting fluid on tool wear in machining AISI 1045 steel. Materials Research Proceedings, 41, 2113–2122. https://doi.org/10.21741/9781644903131-233

Naigade, D. M., Patil, D. H., & Sadaiah, M. (2013). Some investigations in hard turning of AISI 4340 alloy steel in different cutting environments by CBN insert. International Journal of Machining and Machinability of Materials, 14(2), 165–173. https://doi.org/10.1504/IJMMM.2013.055736

Natasha, A. R., Ghani, J. A., Che Haron, C. H., Syarif, J., & Musfirah, A. H. (2016). Temperature at the tool-chip interface in cryogenic and dry turning of AISI 4340 using carbide tool. International Journal of Simulation Modelling, 15(2), 201–212. https://doi.org/10.2507/IJSIMM15(2)1.314

Natasha, A. R., Ghani, J. A., Haron, C. H. C., Syarif, J., Che Haron, C. H., & Syarif, J. (2018). The influence of machining condition and cutting tool wear on surface roughness of AISI 4340 steel. IOP Conference Series: Materials Science and Engineering, 290(1). https://doi.org/10.1088/1757-899X/290/1/012017

Özel, T., & Zeren, E. (2007). Finite element modeling the influence of edge roundness on the stress and temperature fields induced by high-speed machining. International Journal of Advanced Manufacturing Technology, 35(3–4), 255–267. https://doi.org/10.1007/s00170-006-0720-2

Qasim, A., Nisar, S., Shah, A., Khalid, M. S., & Sheikh, M. A. (2015). Optimization of process parameters for machining of AISI-1045 steel using Taguchi design and ANOVA. Simulation Modelling Practice and Theory, 59, 36–51. https://doi.org/10.1016/j.simpat.2015.08.004

Qian, L., & Hossan, M. R. (2007). Effect on cutting force in turning hardened tool steels with cubic boron nitride inserts. Journal of Materials Processing Technology, 191(1–3), 274–278.

https://doi.org/10.1016/j.jmatprotec.2007.03.022

Rahman, H. A., Ghani, J. A., Rasani, M. R. M., Wan Mahmood, W. M. F., Yaaqob, S., & Aziz, M. S. A. (2025). Application of finite element analysis and computational fluid dynamics in machining AISI 4340 steel. Tribology International, 207(February), 110616. https://doi.org/10.1016/j.triboint.2025.110616

Rahman, H. A., Jouini, N., & Ghani, J. A. (2024). A Review of High-Speed Turning of AISI 4340 Steel with Minimum Quantity Lubrication (MQL). Coatings, 1–15.

Sahoo, A. K., & Sahoo, B. (2012). Experimental investigations on machinability aspects in finish hard turning of AISI 4340 steel using uncoated and multilayer coated carbide inserts. Measurement: Journal of the International Measurement Confederation, 45(8), 2153–2165. https://doi.org/10.1016/j.measurement.2012.05.015

Salvatore, F., Saad, S., & Hamdi, H. (2013). Modeling and simulation of tool wear during the cutting process. Procedia CIRP, 8, 305–310. https://doi.org/10.1016/j.procir.2013.06.107

Shalaby, M., & Veldhuis, S. (2018). New observations on high-speed machining of hardened aisi 4340 steel using alumina-based ceramic tools. Journal of Manufacturing and Materials Processing, 2(2). https://doi.org/10.3390/jmmp2020027

Soliman, H. A., Shash, A. Y., El-Hossainy, T. M., & Abd-Rabou, M. (2020). Cutting forces and crater wear prediction in orthogonal cutting using two approaches of finite element modeling. Engineering Reports, 2(10), 1–18. https://doi.org/10.1002/eng2.12240

Sulaiman, S., Roshan, A., & Ariffin, M. K. A. (2013). Finite Element Modelling of the effect of tool rake angle on tool temperature and cutting force during high speed machining of AISI 4340 steel. IOP Conference Series: Materials Science and Engineering, 50(1). https://doi.org/10.1088/1757-899X/50/1/012040

Sumitomo Electric Group. (2023). Indexable Inserts for Turning.

Tiwari, P. K., Kumar, R., Sahoo, A. K., Panda, A., Das, D., & Roy, S. (2020). Performance evaluation of coated cermet insert in hard turning. Materials Today: Proceedings, 26(xxxx), 1941–1947. https://doi.org/10.1016/j.matpr.2020.02.424

Trent, E., & Wright, P. (2000). Metal Cutting 4th Edition. In Angewandte Chemie International Edition, 6(11), 951–952. Butterworth–Heinemann.

Wagri, N. K., Jain, N. K., Petare, A., Das, S. R., Tharwan, M. Y., Alansari, A., Alqahtani, B., Fattouh, M., & Elsheikh, A. (2023). Investigation on the Performance of Coated Carbide Tool during Dry Turning of AISI 4340 Alloy Steel. Materials, 16(2). https://doi.org/10.3390/ma16020668

Wang, B., & Liu, Z. (2014). Investigations on the chip formation mechanism and shear localization sensitivity of high-speed machining Ti6Al4V. International Journal of Advanced Manufacturing Technology, 75(5–8), 1065–1076. https://doi.org/10.1007/s00170-014-6191-y

Wang, L., Wang, W., & Wang, H. (2014). Numerical Analysis on the Factors Affecting the Hydrodynamic Performance for the Parallel Surfaces With Microtextures. Journal of Tribology, 136(April), 1–8. https://doi.org/10.1115/1.4026060

Wu, S., Wang, D., Zhang, J., & Nadykto, A. B. (2022). Study on the Formation Mechanism of Cutting Dead Metal Zone for Turning AISI4340 with Different Chamfering Tools. Micromachines.

Yang, W. H., & Tarng, Y. S. (1998). Design optimization of cutting parameters for turning operations based on the Taguchi method. Journal of Materials Processing Technology, 84(1–3), 122–129. https://doi.org/10.1016/S0924-0136(98)00079-X

Yaqoob, S., Ghani, J. A., Jouini, N., & Juri, A. Z. (2024). Performance Evaluation of PVD and CVD Multilayer-Coated Tools in Machining High-Strength Steel. Coatings, 14(7), 865. https://doi.org/10.3390/coatings14070865

Yaqoob, S., Ghani, J. A., Jouini, N., Juri, A. Z., & Haron, C. H. C. (2024). Multi-objective optimization using Grey Relational Analysis (GRA) for the high-speed orthogonal turning of heat-treated alloy steel. Jurnal Tribologi, 43(July), 1–16.

Zetterberg, M. (2014). A critical overview of machining simulations in ABAQUS. Thèse_Master. www.swerea.se

Zhang, L., Sha, X., Liu, M., Wang, L., & Pang, Y. (2021). Cutting force prediction models by fea and rsm when machining x56 steel with single diamond grit. Micromachines, 12(3). https://doi.org/10.3390/mi12030326